Available online at www.sciencedirect.com
SCIENCE DIRECT®
Optics Communications 246 (2005) 521–528
OPTICS COMMUNICATIONS
www.elsevier.com/locate/optcom

Generation of high-flux ultra-broadband light by bandwidth amplification in spontaneous parametric down conversion

Magued B. Nasr *, Giovanni Di Giuseppe, Bahaa E.A. Saleh, Alexander V. Sergienko, Malvin C. Teich

Departments of Electrical and Computer Engineering and Physics, Quantum Imaging Laboratory, Boston University, 8, Saint Marys Street, Boston, MA 02215, USA [1]

Received 30 September 2004; received in revised form 26 October 2004; accepted 2 November 2004

Abstract

We present a method for generating an ultra-broadband spectrum of spontaneous parametric down conversion (SPDC) that is independent of the thickness of the nonlinear crystal, thereby yielding down-converted photons of high flux. We show that the bandwidth amplification inherent in the SPDC process is maximized at a wavelength where the group-velocity dispersion is minimal. Experimental results demonstrating the broad spectrum produced by this technique are presented.

PACS: 42.50.Dv; 42.65.Lm
Keywords: Quantum optics; Spontaneous parametric down conversion; Quantum optical coherence tomography; Ultra-Broadband

1. Introduction

Ultra-broadband light sources are of great use for applications such as optical coherence tomography (OCT) [1,2], quantum OCT (QOCT) [3,4], and two-photon excitations [5,6]. Several configurations for generating light with an ultra-broadband spectrum have been proposed and experimentally demonstrated [2,7,8]. In this letter, we show that such an ultra-broadband spectrum can be produced via the nonlinear optical process of spontaneous parametric down conversion (SPDC).

In the process of SPDC [9], a light source pumps a nonlinear optical crystal (NLC). The

[1] http://www.bu.edu/qil.

* Corresponding author. Tel.: +1 6173539943; fax: +1 6173530101.
E-mail addresses: mboshra@yahoo.com (M.B. Nasr), besaleh@bu.edu (B.E.A. Saleh).

0030-4018/$ - see front matter © 2004 Elsevier B.V. All rights reserved.
doi:10.1016/j.optcom.2004.11.008

nonlinear interaction inside the crystal leads to the annihilation of a high-frequency pump photon and the creation of a pair of lower-frequency photons, traditionally called signal and idler. The dependence of the signal and idler's frequencies on the frequency of the pump is governed by the phase-matching conditions, whose nonlinearity can be exploited for bandwidth amplification, so that a narrow-band pump can result in the generation of ultra-broadband signal and idler spectra. This effect is maximal at the down-conversion wavelength for which the group-velocity dispersion (GVD) of the NLC cancels. Under these conditions of large-bandwidth amplification, the crystal thickness does not play a role in determining the bandwidth. Thus, thick crystals can be used, thereby yielding a high flux of down converted photons.

2. Perfect phase matching

The phase-matching conditions, which comprise energy and momentum conservation, are given by [9]:

$$\omega_s + \omega_i = \omega_p, \tag{1}$$

$$\mathbf{k}_s(\omega_s) + \mathbf{k}_i(\omega_i) = \mathbf{k}_p(\omega_p), \tag{2}$$

where the subscript p refers to the pump, and the subscripts s and i refer to the signal and idler down-converted photons, respectively. The quantities ω_j and $\mathbf{k}_j$, with j = p, s, and i, are the angular frequencies (henceforth called frequencies) and wave vectors inside the NLC, respectively. These ideal conditions are applicable for an infinitely thick NLC.

In the special case of collinear type-I SPDC, the down-converted photons co-propagate with the pump and have the same polarization, which is orthogonal to that of the pump. The momentum-conservation condition, Eq. (2), reduces to a scalar equation with each wave vector replaced by its magnitude,

$$k_p(\omega_p) = \frac{\omega_p n_e(\omega_p, \theta_{cut})}{c},$$

$$k_{s,i}(\omega_{s,i}) = \frac{\omega_{s,i} n_o(\omega_{s,i})}{c}. \tag{3}$$

The quantity $n_e(\omega_p,\theta_{cut})$ is the extraordinary refractive index of the birefringent NLC experienced by the pump, and $n_o(\omega_{s,i})$ is the ordinary refractive index for the signal and idler waves. These refractive indices can be computed using the Sellmeier equations for the specific NLC material [10]. The parameter θ_{cut} is the "cut angle" of the NLC, and c is the speed of light in vacuum.

For a given pump frequency ω_p and crystal cut angle θ_{cut}, the signal and idler frequencies, ω_s and ω_i, are computed using Eqs. (1)–(3). A special case is degenerate collinear down-conversion, where the signal and idler have the same frequency, $\omega_{s,i} = \omega_{p_o}/2$ for $\omega_p = \omega_{p_o}$. For example pumping a lithium iodate ($LiIO_3$) NLC of $\theta_{cut} = 39.8°$ with a wavelength $\lambda_{p_o} = 2\pi c/\omega_{p_o} = 420$ nm, will result in degenerate collinear down-converted photons at $\lambda_o = 2\lambda_{p_o}$.

We study the effect of changes in the pump frequency on the frequency of the down-converted photons by varying ω_p about the fixed frequency ω_{p_o}. A change in the pump frequency by a value $\Delta\omega_p$, such that $\omega_p = \omega_{p_o} + \Delta\omega_p$, results in a frequency change $\Delta\omega_{s,i}$ of the collinear signal and idler photons such that $\omega_{s,i} = \omega_{p_o}/2 + \Delta\omega_{s,i}$, subject to $\Delta\omega_s + \Delta\omega_i = \Delta\omega_p$. An approximate analytic expression for the dependence of $\Delta\omega_{s,i}$ on $\Delta\omega_p$ can be obtained by expanding the wave numbers to second order: $k_j(\omega_j) \approx k_j^o + k_j'\Delta\omega_j + \frac{1}{2}k_j''(\Delta\omega_j)^2$, where j again stands for p, s, and i. We expand the pump's wave number around ω_{p_o}, and the signal and idler wave numbers around the degenerate frequency $\omega_{p_o}/2$. The quantities k_j' and k_j'' represent the inverse of the group velocity and the GVD experienced by each photon as it travels through the NLC, respectively. Using this expansion, the frequency deviation of the signal/idler is approximated by

$$\Delta\omega_{s,i} \approx \frac{\Delta\omega_p}{2} \pm \sqrt{\gamma\Delta\omega_p}, \tag{4}$$

where we define a spectral-gain parameter γ as

$$\gamma = \frac{k_p' - k'}{k''}, \tag{5}$$

where k' stands for k_s' or k_i' which are equal, and likewise for k''. Note that the spectral-gain parameter is positive since we're operating in the normal

dispersion region of the material, and would grow to infinity, within this approximation, at down-conversion wavelengths for which the GVD cancels.

A plot of the dependence of $\Delta\omega_{s,i}$ on $\Delta\omega_p$ is shown in Fig. 1 for $LiIO_3$. The solid curve is the exact solution to the phase-matching conditions using the Sellmeier equations, whereas the dashed curve is the approximate solution given in Eq. (4). The two curves clearly match for low values of $\Delta\omega_p$, but the deviation becomes perceptable for large $\Delta\omega_p$. In the inset of Fig. 1, we plot the dependence of the spectral-gain parameter γ on the wavelength of the signal and idler photons, $\lambda_{s,i}$. In plotting γ, the cut angle of the NLC was computed to ensure collinear-degenerate down conversion.

As is evident in Fig. 1, a small change in the pump frequency $\Delta\omega_p$ can lead to a large change of the frequency of down conversion $\Delta\omega_{s,i}$. For example a change of $\Delta\omega_p = 2\times10^{13}$ rad/s, corresponding to a wavelength change of 2 nm (from $\lambda_p = 420$ to 418 nm), results in a change in the down-conversion frequency of $\Delta\omega_{s,i} = \pm24\times10^{13}$ rad/s, a value that is 24 times greater than $\Delta\omega_p$.

Based on these results, it is clear that a non-monochromatic pump with a spectrum spanning the frequencies between ω_{p_o} and $\omega_{p_o} + \Delta\omega_p$ will generate down-converted photons with a spectrum covering the range $\omega_{p_o}/2 \pm \Delta\omega_{s,i}$, yielding a substantial bandwidth gain. The bandwidth gain, $\Delta\omega_{s,i}/\Delta\omega_p$, increases monotonically with $\sqrt{\gamma}$ and decreases with $\sqrt{\Delta\omega_p}$ as shown in Eq. (4). A negative value of $\Delta\omega_p$ does not result in collinear phase matching.

3. Quantum mechanical treatment

We now proceed to show that this acquired benefit of bandwidth amplification, which has heretofore been described in the context of an infinitely thick crystal (perfect phase matching), is, in fact, independent of the NLC thickness. For a broadband pump (e.g., a pulsed laser) pumping a type-I NLC of finite thickness, and assuming a uniform transverse distribution (i.e., a plane-wave), the down-converted two-photon state is given by [11]

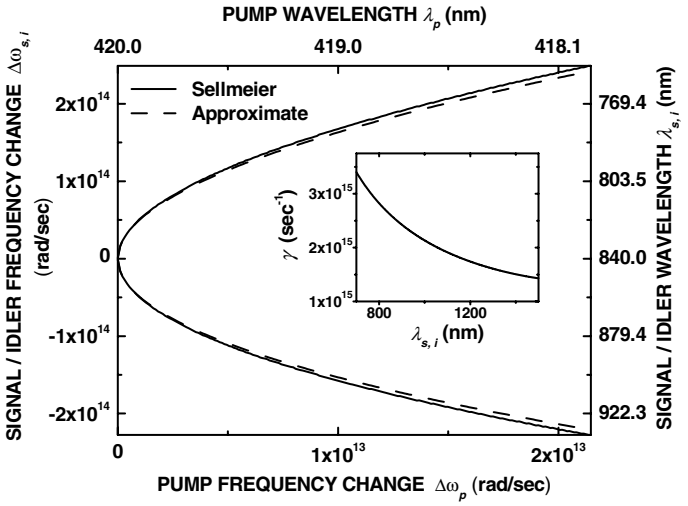

Fig. 1. Change in the down-conversion angular frequency, $\Delta\omega_{s,i}$, versus the change in the pump angular frequency, $\Delta\omega_p$, assuming perfect phase matching, in accordance with Eqs. (1)–(3). The solid curve is plotted using the exact wave-number values computed from the Sellmeier equations for $LiIO_3$, while the dashed curve is plotted using Eq. (4), obtained from a second-order approximation of the wave numbers. The zero point on the ordinate corresponds to the degenerate case where a monochromatic pump of wavelength $\lambda_p = 420$ nm produces signal and idler photons at $\lambda_{s,i} = 840$ nm. The top abscissa is the wavelength of the pump that corresponds to the change in angular frequency indicated on the bottom abscissa. The right ordinate indicates the signal and idler wavelength corresponding to the frequency shift indicated on the left ordinate. In the inset we plot the spectral gain parameter γ, appearing in Eq. (5), as a function of $\lambda_{s,i}$.

$$|\psi\rangle = \int \mathrm{d}\omega_s \int \mathrm{d}\omega_i E_p(\omega_s + \omega_i)\Phi(\omega_s, \omega_i)\,|\omega_s\rangle\,|\omega_i\rangle. \tag{6}$$

The function $\Phi(\omega_s,\omega_i)$ is the phase-matching function given by

$$\Phi(\omega_s, \omega_i) = \mathrm{sinc}\{[k_s(\omega_s)\alpha(\omega_s) + k_i(\omega_i)\alpha(\omega_i) - k_p(\omega_s + \omega_i)]L/2\}, \tag{7}$$

where L is the NLC thickness, $\mathrm{sinc}(x) = \sin(x)/x$, $E_p(\omega)$ is the Fourier transform of the temporal distribution of the pulsed pump, and $|\omega_{s,i}\rangle$ is a one-photon Fock state at the signal/idler frequency. The parameter $\alpha(\omega_{s,i})$ is given by

$$\alpha(\omega_{s,i}) = \sqrt{n_o^2(\omega_{s,i}) - \sin^2(\theta_{out})}/n_o(\omega_{s,i}), \tag{8}$$

where θ_{out} is the angle between the non-collinear down-converted photon beams and the pump, measured outside the NLC.

The power spectral densities $\mathscr{S}_s(\omega_s)$ and $\mathscr{S}_i(\omega_i)$ of the individual signal and idler photons (singles spectra), given by

$$\mathscr{S}_{s,i}(\omega_{s,i}) = \int \mathrm{d}\omega_{i,s}\,|E_p(\omega_s + \omega_i)\Phi(\omega_s, \omega_i)|^2, \tag{9}$$

are identical because of the underlying symmetry of the function $\Phi(\omega_s,\omega_i)$. In type-II SPDC, on the other hand, the signal and idler are orthogonally polarized and do not, in general, have identical spectra [11].

4. Independence of singles-spectrum bandwidth on NLC thickness

Using Eqs. (3), (7), (8), and (9) we plot the singles spectra in Fig. 2. We assume a Gaussian pump, $E_p(\omega) = (1/\sqrt{2\pi}\sigma)\exp(-(\omega - \omega_{p_o})^2/2\sigma^2)$, whose spectral intensity, $|E_p(\omega)|^2$, has a FWHM equal to $2\sqrt{\ln 2}\sigma$. In our computations we assume a center wavelength $\lambda_p = 420$ nm and a spectral width $\sigma = 3\times10^{13}$ rad/s. Such a pump can be obtained by doubling the output of a pulsed Ti:Al_2O_3 laser operating at $\lambda_o = 840$ nm. We present plots for three $LiIO_3$ nonlinear crystals of different thicknesses, $L = 0.1$, 1.0, and 10 mm; we have chosen $\theta_{cut} = 39.8°$. For comparison, we plot the spectral intensity $|E_p(\omega)|^2$ of a Ti:Al_2O_3 pulsed laser before doubling. It is clear from Fig. 2 that the singles spectrum is effectively *independent of the NLC thickness*.

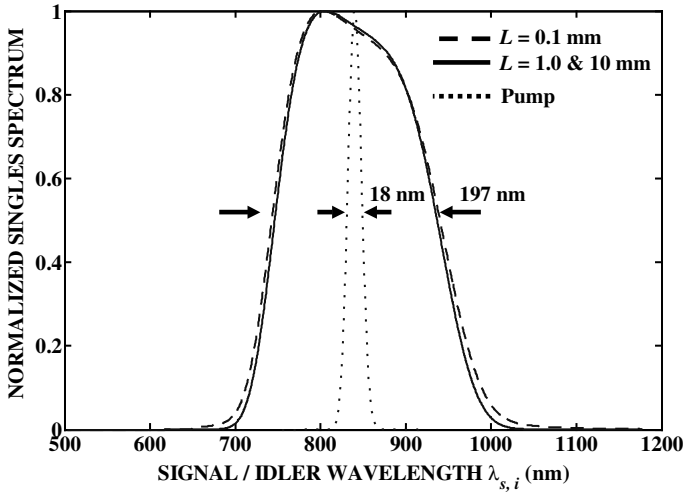

Fig. 2. Calculated normalized singles spectrum for three values of the nonlinear crystal thickness: $L = 0.1$ mm (dashed); $L = 1.0$ mm and 10 mm (solid). We assume a pump with a Gaussian spectrum of spectral width $\sigma = 3\times10^{13}$ rad/s centered around $\lambda_p = 420$ nm. Such a pump could be obtained by doubling the output of a pulsed Ti:Al_2O_3 laser operating at $\lambda_o = 840$ nm which would have a spectral intensity $|E_p(\omega)|^2$, as shown by the dotted curve. The plots represent results for a $LiIO_3$ NLC with $\theta_{cut} = 39.8°$, as used in Fig. 1.

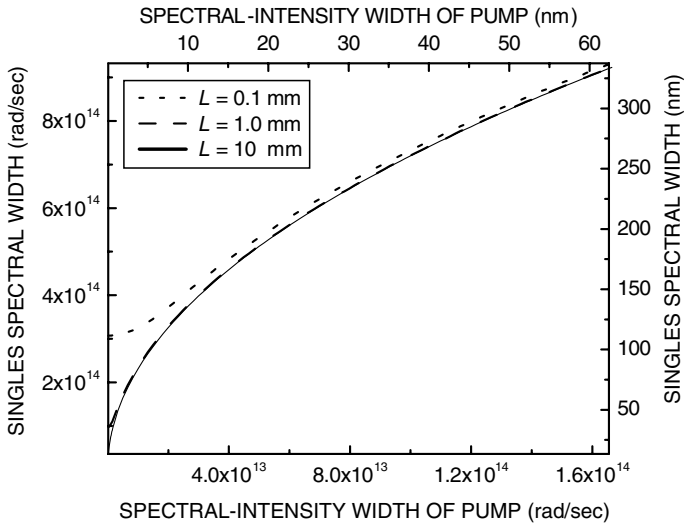

Fig. 3. The FWHM of the singles spectrum vs. the FWHM of the pump's spectral intensity, $|E_p(\omega)|^2$, for three nonlinear crystal thicknesses: $L = 0.1$ mm (dotted), $L = 1$ mm (dashed), and $L = 10$ mm (solid). We assume a pump with a Gaussian spectrum centered around $\lambda_p = 420$ nm. Such a pump could be obtained by doubling the output of a pulsed Ti:Al_2O_3 laser operating at $\lambda_o = 840$ nm. The bottom abscissa is the FWHM of the Ti:Al_2O_3 spectral intensity in rad/s, whereas the top abscissa is the same quantity in nm. The left ordinate is the FWHM of the spectrum of down conversion (singles spectrum) in rad/s while the right ordinate is the same quantity in nm.

In Fig. 3 we plot the FWHM of the singles spectra as a function of the FWHM of the pump's spectral intensity, $|E_p(\omega)|^2$. It is clear that for a pump with sufficiently broad spectrum, the effect of the NLC thickness is negligible. This confirms previously obtained theoretical results [12], and is of great importance for the production of high-flux broadband down-converted photons. For a monochromatic pump, the NLC thickness plays the dominant role in determining the singles spectra. In this case thinner NLCs generate broader singles spectra but have the disadvantage of low photon flux.

The singles spectrum depends on the overlap of the two functions $E_p(\omega_s + \omega_i)$ and $\Phi(\omega_s,\omega_i)$, as shown in Eq. (9). We plot these two functions, along with their product, in Fig. 4. The pump spectrum $E_p(\omega_s + \omega_i)$, shown in the leftmost plot, is a band extending parallel to the $\omega_s = -\omega_i$ line, which has an infinite length and a thickness that depends on the pump spectral width σ. The width of the phase-matching function $\Phi(\omega_s,\omega_i)$, shown in the center plot, is determined by the crystal thickness L; its curvature is governed by the dispersion properties of the material. If the curvature of $\Phi(\omega_s,\omega_i)$ is negligible, the product of E_p and Φ continues to stretch over an infinite length. It is apparent from Eq. (9) that the singles spectra will then have infinite width since they are simply the projection of $|E_p\Phi|^2$ on the axes ω_s and ω_i. This result is independent of the width of either of the two functions. The effect of curvature in the phase-matching function is to reduce the overlap between E_p and Φ, thereby leading to a reduced singles-spectrum bandwidth, as exemplified in the rightmost plot of Fig. 4. Such a curvature plays a far larger role than crystal thickness in determining the singles spectra.

This effect can be examined quantitatively by expanding the wave numbers $k_j(\omega_j)$ to second order, as in the derivation of Eq. (4). The phase-matching function $\Phi(\omega_s,\omega_i)$ in Eq. (7) can then be written as

$$\Phi(\omega_s,\omega_i) \approx \mathrm{sinc}\{[A(\Delta\omega_s + \Delta\omega_i) + B(\Delta\omega_s + \Delta\omega_i)^2 - C(\Delta\omega_s\Delta\omega_i)]L/2\}, \quad (10)$$

with $A = k' - k'_p$, $B = (k'' - k''_p)/2$, and $C = k''$. If the GVD at the wavelength of the down-converted

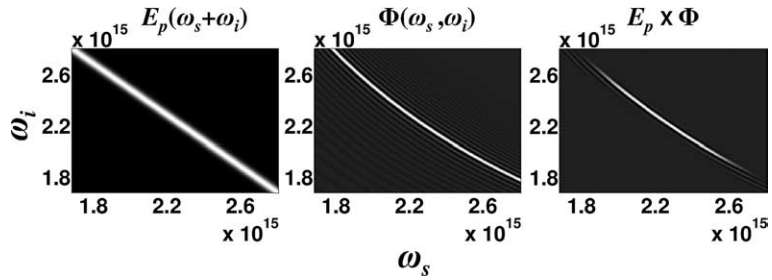

Fig. 4. Plots of the pump spectrum $E_p(\omega_s + \omega_i)$ (left); the phase-matching function $\Phi(\omega_s,\omega_i)$ (middle); and the product of the two functions, $E_p(\omega_s + \omega_i) \times \Phi(\omega_s,\omega_i)$ (right).

photons vanishes, i.e., $k'' = 0$, $\Phi(\omega_s,\omega_i)$ depends only on $(\Delta\omega_s + \Delta\omega_i)$ so that there is no curvature and therefore an infinite singles spectrum. This result is analogous to that obtained in Eq. (5), in which the spectral gain parameter γ becomes infinite for vanishing GVD. In this limiting case, higher-order dispersion terms come into play. It is gratifying that, within a second-order approximation, these two routes (perfect phase matching and quantum treatment) lead to that same result.

In the theoretical exposition presented thus far, a plane-wave pump has been assumed. The use of a spatially non-uniform pulsed pump, such as a focused pump, was theoretically studied in [13]. According to [13], the effect of the pump's spatial distribution comes into play when the ratio of the pump's beam waist to the crystal's length violates a certain condition. In the experimental work presented in the following section we do not violate this condition.

5. Experimental results

Finally we present the results of an experiment that confirms the theory considered above. The experimental setup is shown in Fig. 5. The output of a pulsed Ti:Al_2O_3 laser (pumped by a monochromatic Ar-ion laser) having a FWHM of 18 nm, centered about the wavelength 840 nm, is doubled to 420 nm and is used to pump $LiIO_3$ crystals of different thicknesses. The laser beam is collimated to a spot diameter of ≈2 mm at the crystal input. The down-converted photons are emitted in two non-collinear beams, denoted 1 and 2, that make an output angle $\theta_{out} = 8°$ with respect to the pump. The photons in beam 1 are discarded and the autocorrelation function of the photons in beam 2 are obtained using a Michelson interferometer which consists of mirrors M_1 and M_2, beam splitter BS, and the single-photon-counting detector D. A 4.5-mm aperture A, and a long-pass filter F with cutoff at 625 nm are placed in front of the detector to minimize background leakage. The temporal delay τ is swept and the singles rate is recorded, forming the autocorrelation function $I(\tau)$.

In Figs. 6(a) and (b) we plot the measured autocorrelation function for the down-converted light produced in a 1-mm and a 12-mm thick $LiIO_3$

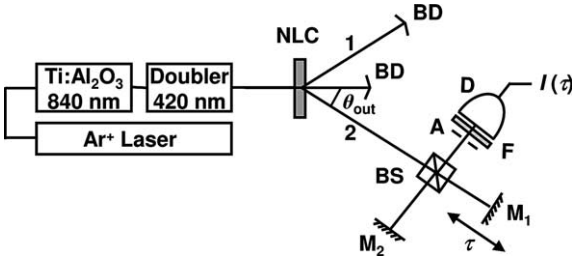

Fig. 5. Experimental arrangement for measuring the autocorrelation function $I(\tau)$ for the down-converted photons. A monochromatic Ar^+-ion laser pumps a pulsed Ti:Al_2O_3 laser generating an 18-nm-wide, full width at half maximum (FWHM), spectrum centered about the wavelength 840 nm. The output of the Ti:Al_2O_3 is doubled to 420 nm and is used to pump $LiIO_3$ crystals of different thicknesses. The laser beam is collimated to a spot diameter of ≈2 mm at the crystal input. The down-converted photons are emitted in a non-collinear fashion making an angle $\theta_{out} = 8°$ with the pump. BD stands for beam dump, BS for beam splitter, M for mirror, A for 4.5-mm aperture, F for long-pass filter with cutoff at 625 nm, and D for single-photon-counting detector (EG&G, SPCM-AQR-15). The quantity τ represents a temporal delay.

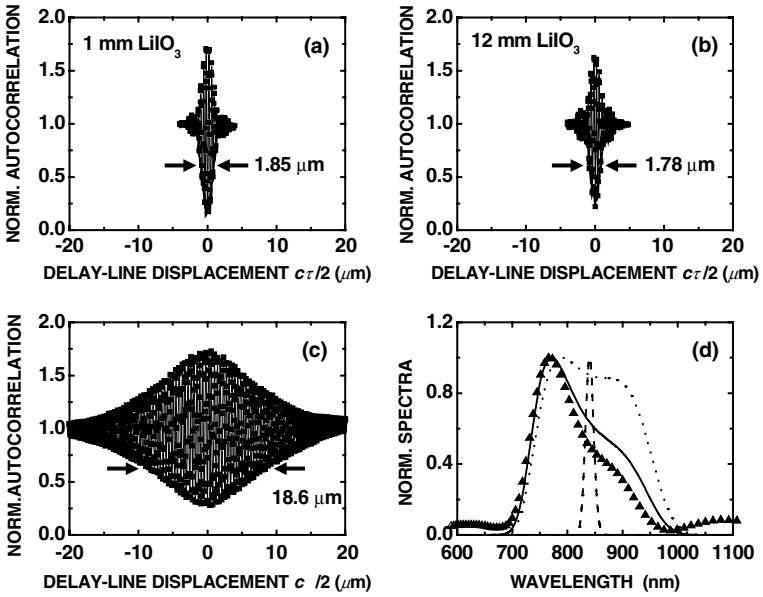

Fig. 6. Experimental results. Autocorrelation of a beam of down-converted light produced in: (a) a 1-mm thick $LiIO_3$ NLC; (b) a 12-mm thick $LiIO_3$ NLC. Note that the widths of the two functions are quite similar. (c) Autocorrelation of the Ti:Al_2O_3 pump pulse. Note that it is approximately a factor of 10 broader than the autocorrelation functions in (a) and (b). (d) Calculated spectrum of the down conversion (dotted curve); calculated spectrum of the down conversion multiplied by the spectral response of the single-photon-counting detector which peaks at 700 nm (solid curve); experimental spectrum of the Ti:Al_2O_3 pulsed laser pump (dashed curve); and experimental spectrum of down conversion obtained by taking the Fourier transform of the autocorrelation function in (b) (triangles). The theoretical (solid curve) and experimental (triangles) spectra are in good accord.

NLC, respectively. The widths of the two autocorrelation functions are seen to be quite similar in spite of the substantial difference in the thickness of the crystals. In Fig. 6(c) we plot the autocorrelation function of the Ti:Al_2O_3 output, which is obviously broader than the down-conversion autocorrelation functions in Figs. 6(a) and (b). Since the Fourier transform of the autocorrelation function is the singles spectrum, it is clear that we have experimentally generated ultra-broadband SPDC with a bandwidth amplification factor of $\approx$10.

In Fig. 6(d), the dashed, dotted, and solid curves represent, respectively, the spectrum of the Ti:Al_2O_3 output (the Fourier transform of Fig. 6(c)), the calculated singles spectrum (from Eqs. (7)–(9)), and the calculated singles spectrum multiplied by the spectral response of the single-photon-counting detector, which has its peak response at 700 nm (EG&G, SPCM-AQR-15). The experimental singles spectrum (triangles) is the Fourier transform of the autocorrelation function shown in Fig. 6 (b). It is apparent that the theoretical (solid curve) and experimental (triangles) singles spectrum are in good accord, thereby confirming the validity of the theory.

Acknowledgements

This work was supported by the National Science Foundation; by the Center for Subsurface Sensing and Imaging Systems (CenSSIS), an NSF Engineering Research Center; and by the David & Lucile Packard Foundation.

References

[1] A.F. Fercher, W. Drexler, C.K. Hitzenberger, T. Lasser, Rep. Prog. Phys. 66 (2003) 239.
[2] B. Povazay, K. Bizheva, A. Unterhuber, B. Hermann, H. Sattmann, A.F. Fercher, W. Drexler, A. Apolonski, W.J. Wadsworth, J.C. Knight, P.St.J. Russell, M. Vetterlein, E. Scherzer, Opt. Lett. 27 (2002) 1800.

[3] A.F. Abouraddy, M.B. Nasr, B.E.A. Saleh, A.V. Sergienko, M.C. Teich, Phys. Rev. A 65 (2002) 053817.
[4] M.B. Nasr, B.E.A. Saleh, A.V. Sergienko, M.C. Teich, Phys. Rev. Lett. 91 (2003) 083601.
[5] I. Abram, R.K. Raj, J.L. Oudar, G. Dolique, Phys. Rev. Lett. 57 (1986) 2516.
[6] M.C. Teich, B.E.A. Saleh, Ceskoslovenski casopis pro fyziku 47 (1997) 3.
[7] S. Coen, A.H.L. Chau, R. Leonhardt, J.D. Harvey, J.C. Knight, W.J. Wadsworth, P.St.J. Russell, J. Opt. Soc. Am. B 19 (2002) 753.
[8] Y. Wang, Y. Zhao, J.S. Nelson, Z. Chen, R.S. Windeler, Opt. Lett. 28 (2003) 182.
[9] L. Mandel, E. Wolf, Optical Coherence and Quantum Optics, Cambridge, New York, 1995 (Chapter 22).
[10] M. Bass (Ed.), Handbook of Optics, vol. II, 2nd ed., McGraw-Hill, New York, 1995 (Chapter 33).
[11] W.P. Grice, I.A. Walmsley, Phys. Rev. A 56 (1997) 1627.
[12] A. Joobeur, B.E.A. Saleh, T.S. Larchuk, M.C. Teich, Phys. Rev. A 53 (1996) 4360.
[13] A.B. U'ren, K. Banaszek, I.A. Walmsley, Quantum Inform. Comput. 3 (2003) 480.